Journal of Hazardous Materials 448 (2023) 130874

Contents lists available at ScienceDirect

Journal of Hazardous Materials

journal homepage: www.elsevier.com/locate/jhazmat

Cobalt oxide functionalized ceramic membrane for 4-hydroxybenzoic acid degradation via peroxymonosulfate activation

Rajan Arjan Kalyan Hirani [a,1], Hong Wu [a,1], Abdul Hannan Asif [a], Nasir Rafique [a], Lei Shi [b], Shu Zhang [b], Zhentao Wu [c], Lai-Chang Zhang [d], Shaobin Wang [e], Yu Yin [f], Martin Saunders [g], Hongqi Sun [a,*]

[a] School of Science, Edith Cowan University, 270 Joondalup Drive, Joondalup, WA 6027, Australia
[b] College of Materials Science and Engineering, Nanjing Forestry University, 210037 Nanjing, China
[c] Aston Institute of Materials Research, School of Engineering and Applied Science, Aston University, B4 7ET Birmingham, UK
[d] School of Engineering, Edith Cowan University, 270 Joondalup Drive, Joondalup, WA 6027, Australia
[e] School of Chemical Engineering and Advanced Materials, The University of Adelaide, Adelaide, SA 5005, Australia
[f] School of Environmental and Chemical Engineering, Jiangsu University of Science and Technology, Zhenjiang 212003, China
[g] Centre for Microscopy, Characterisation and Analysis (CMCA), University of Western Australia, Perth, WA 6009, Australia

HIGHLIGHTS

- Co_3O_4 integrated ceramic membranes were fabricated via a simple ball-milling and sintering approach.
- Catalytic oxidation of 4-hydroxybenzoic acid was conducted in a crossflow membrane reactor.
- Both $SO_4^{\bullet-}$ and $^{\bullet}OH$ were present in the degradation with $SO_4^{\bullet-}$ as the dominant species.
- Anti-fouling performance of the membranes was observed.

GRAPHICAL ABSTRACT

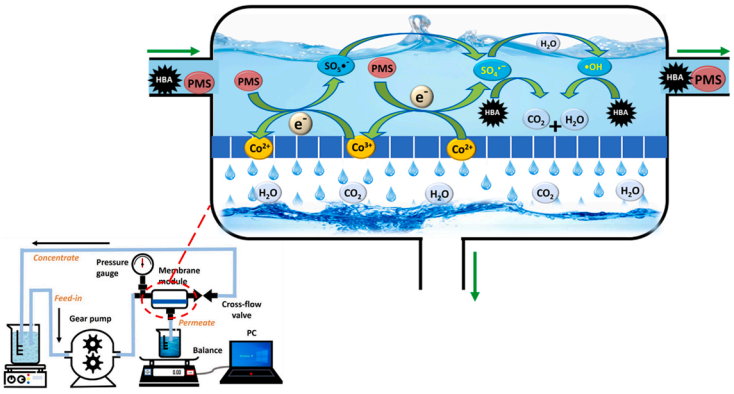

ARTICLE INFO

Editor: Haizhou Liu

Keywords:
Catalytic membrane
Co_3O_4
Sulfate radicals
Catalytic oxidation
AOPs

ABSTRACT

Membrane separation and sulfate radicals-based advanced oxidation processes (SR-AOPs) can be combined as an efficient technique for the elimination of organic pollutants. The immobilization of metal oxide catalysts on ceramic membranes can enrich the membrane separation technology with catalytic oxidation avoiding recovering suspended catalysts. Herein, nanostructured Co_3O_4 ceramic catalytic membranes with different Co loadings were fabricated via a simple ball-milling and calcination process. Uniform distribution of Co_3O_4 nanoparticles in the membrane provided sufficient active sites for catalytic oxidation of 4-hydroxybenzoic acid (HBA). Mechanistic studies were conducted to determine the reactive radicals and showed that both $SO_4^{\bullet-}$ and $^{\bullet}OH$ were

* Corresponding author.
E-mail address: h.sun@ecu.edu.au (H. Sun).
[1] Co-first authors.

https://doi.org/10.1016/j.jhazmat.2023.130874
Received 26 October 2022; Received in revised form 18 December 2022; Accepted 24 January 2023
Available online 25 January 2023

present in the catalytic process while $SO_4^{\bullet-}$ plays the dominant role. The anti-fouling performance of the composite Co@Al_2O_3 membranes was also evaluated, showing that a great flux recovery was achieved with the addition of PMS for the fouling caused by humic acid (HA).

Environmental implications

Discharge of pharmaceuticals and personal care products (PPCPs) in wastewater has been inevitable in the past few years. These PPCPs have shown adverse impacts on human and ecological health and therefore, it is urgent to exploit sustainable technologies to mitigate these contaminants. Advanced oxidation processes (AOPs) have shown promising results in the oxidation of PPCPs to less toxic compounds but have a major challenge in catalyst recovery and reusability. Herein, AOPs combined with membrane technology has been implemented for the degradation of a paraben. It shows that AOPs can be empowered by membrane technology for environmental remediation.

Data availability

Data will be made available on request.

1. Introduction

The increasing environmental and health impacts of water pollution caused by rapid modernization, industrialization and urbanization have become one of the most perennial issues worldwide. With the greater demand for clean water sources, various water treatment technologies have been developed to eliminate the micro-pollutants and contaminants discharged to natural water bodies [1]. 4-hydroxybenzoic acid (HBA), a phenolic derivative of benzoic acid and an intermediate compound of parabens, is one such example of PPCPs due to its lower biodegradability nature and high chemical oxygen demand (COD). Such properties have made HBA resistant to natural degradation, hence creating an urgent need for sustainable and effective remediation technologies. Among these treatment strategies, advanced oxidation processes (AOPs), which rely on highly reactive species, have been considered the most efficient protocols for the removal of persistent organic pollutants that are difficult to be removed by conventional physical, chemical, or biological processes [2]. In the process, $^{\bullet}OH$ and $SO_4^{\bullet-}$ are the two primary free radical species and can be generated from the activation of hydrogen peroxide (H_2O_2), ozone (O_3), persulfate (PS) and peroxymonosulfate (PMS). The higher redox potentials of $^{\bullet}OH$ and $SO_4^{\bullet-}$ compared to their parent peroxides make these free radicals ideal for the quick degradation and complete mineralization of recalcitrant organic compounds [3]. It is known that $^{\bullet}OH$ is highly oxidative with an oxidation potential of 2.7 V, and can efficiently mineralize the contaminants into water, carbon dioxide, ions, and mineral acids [4]. However, $^{\bullet}OH$ is ineffective for some compounds, such as acetic and oxalic acids, acetone, and chloride derivatives [5]. Recently, sulfate radicals-based advanced oxidation processes (SR-AOPs) have drawn growing attention. Compared to their $^{\bullet}OH$ counterparts, $SO_4^{\bullet-}$ have a higher oxidation potential (2.5–3.1 V vs 2.8 V), longer half-life, less selectivity, and wider capable pH range (pH 2–8 for $SO_4^{\bullet-}$, and pH 3–4 for $^{\bullet}OH$) [6]. Therefore, SR-AOPs are recognized as a promising alternative for conventional AOPs such as Fenton, photocatalysis and catalytic ozonation processes.

Both peroxymonosulfate (PMS) and persulfate have a superoxide O−O bond which can be easily dissociated to form reactive radicals [7]. Compared to PS, the activation of PMS can produce both $^{\bullet}OH$ and $SO_4^{\bullet-}$ radicals, indicating the integrated properties [5]. PMS can be activated by various methods such as heat, UV, metal ions, metal oxides, and metal-free catalysts [8]. Heat and UV light are effective for the activation PMS, however, the demand for energy input (additional heating units or light sources) is high, making them relatively expensive and unsuitable for large-scale applications [9]. Homogeneous activation of PMS by using transition metal ions such as Co(II), Mn (II), and Ru(II) is another technique which has demonstrated good performance [10]. However, the direct discharge of the metal ions will bring about secondary contamination to the environment. To overcome this problem, heterogeneous activation of PMS using metal oxide catalysts has drawn increasing attention. Cobalt oxides and manganese oxides have been reported to be excellent heterogeneous catalysts in PMS activation. However, metal leaching of toxic cobalt and manganese ions is still present in the solution after the reaction [11,12]. Carbonaceous catalysts such as carbon nanotubes (CNTs) [4], reduced graphene oxide [13], and nanodiamonds (NDs) [14] are alternative solutions to the metal leaching problem. However, the drawbacks of low durability and high cost have restricted the application of metal-free catalysts in SR-AOPs for wastewater remediation [15].

The combination of SR-AOPs and membrane filtration technology has emerged as an alternative to heterogeneous catalysis. There are two approaches for PMS/membrane combination: (a) SR-AOPs are used as a pre-treatment, and (b) a catalytic membrane is used for $SO_4^{\bullet-}$ activation. First, in the SR-AOPs pre-treatment technology, the membrane itself can act as a barrier for both catalysts and pollutants, making the heterogeneous catalysts of transition metal oxides easy to be collected and reused. Cheng et al. employed Fe (II)/PMS degradation as a pre-treatment method for membrane fouling control. The combination of Fe (II)/PMS degradation with coagulation as pre-treatment for membrane fouling alleviation was also investigated [16-18]. Besides the ferrous ions, metal oxide nanoparticles can also be used for membrane fouling mitigation. The performances of CuO/PMS, Co_3O_4/PMS and MnO_2/PMS systems for the control of membrane fouling caused by natural organic matters (NOMs) were compared by Cheng et al., who found that both reversible and irreversible fouling can be dramatically alleviated in CuO/PMS and Co_3O_4/PMS. Whereas in the MnO_2/PMS system, the irreversible fouling mitigation was limited [19]. Secondly, catalysts can be integrated into the membrane support to achieve the synergistic function of both separation and catalytic oxidation. Recently, metal oxide integrated membranes have been used in SR-AOPs/composite catalytic membrane processes [20-23]. In other works, metal-free catalysts were incorporated in membrane supports in SR-AOP/membrane systems [24,25]. Cobalt oxides are frequently studied in the heterogeneous activation of PMS. Generally, in homogeneous transition metal ions/PMS systems, the Co (II)/PMS system demonstrates the best activity among various metal ions (Mn (II), Ce (III), Ni (II), Fe (II), V (III), and Ru (III))/PMS systems [26,27]. However, Co ions remaining in treated water can cause acute and chronic health problems and the LD_{50} value for soluble Co salts was reported between 150 and 500 mg kg^{-1} [28].

Herein, a simple ball-milling and calcination method was used to prepare cobalt oxide functionalized ceramic membranes for the catalytic oxidation of HBA with PMS. Compared with other preparation methods of Co integrated catalytic membranes [29-32] using a Co precursor suspension, the ball-milling and calcination method employed powdered cobalt oxides as part of the aggregate of the ceramic membranes, making the Co amount in the membrane accurately controllable. Morphological characterization of the Co@Al_2O_3 membranes indicated a uniform distribution of Co_3O_4 on every single Al_2O_3 particle in the whole membrane owing to the planetary ball-milling process. The high level of uniform Co distribution in the membrane endowed a prominent PMS activation performance with the dispersive Co reactive sites.

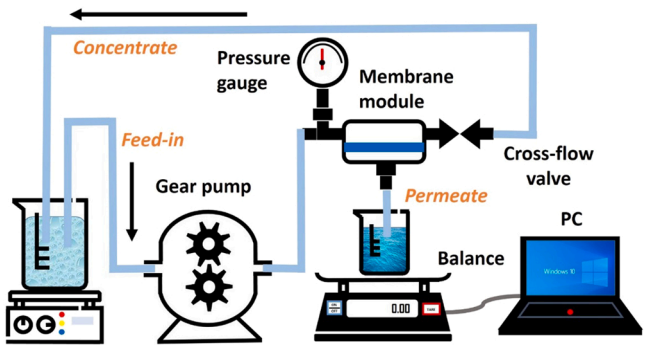

Fig. 1. Membrane reactor system set-up.

Fouling alleviation tests on the Co@Al_2O_3 catalytic membrane/PMS system were also performed. Results showed a significant improvement for the Co@Al_2O_3 membrane at the presence of PMS when compared with that without PMS. Finally, the possible ROS generation mechanism was speculated based on the EPR and reactive radicals quenching tests.

2. Experimental

2.1. Reagents and materials

All the reagents and materials used in this study have been listed and described in the supplementary information as Text S1.

2.2. Synthesis of cobalt oxides

Co_3O_4 nanocubes were synthesized by a modified solvent-thermal process reported by Song et.al [33]. Typically, 1.416 g of cobalt (II) acetate tetrahydrate was completely dissolved in 30 mL ethanol under continuous stirring for 2 h. The subsequent solution was then transferred into a 50 mL autoclave and placed in an oven at 90 °C for 2 h followed by natural cool down. The resulting pink precipitate was washed by ethanol several times and dried overnight. The dried powder was annealed in a tubular furnace at 200 °C for 6 h under a continuous flow of air.

2.3. Fabrication of membranes

Co_3O_4 integrated ceramic membranes were synthesized as follows: Co_3O_4 nanocubes (1, 2, 5, or 10 wt%), Al_2O_3 nanoparticles, PVA (1%) and glycerol (1.5%) were first mixed and ground using a planetary ball milling procedure (Fritsch, Pulverisette 6, Germany), as reported in detail in our earlier work [22]. The composite membrane samples with different Co_3O_4 loadings were then denoted to Co-1, Co-2, Co-5, and Co-10, respectively. The after-milled powders were then sieved in an automatic sieve shaker to obtain uniform size distribution. The resulting powders were then pressed in a membrane mould by a hydraulic press under a pressure of 5 bar to produce membranes and then dried for 12 h at 60 °C. Thereafter, the as-prepared membranes were calcined at 1050 °C to obtain the final membranes with a diameter of 28 mm and thickness of 3.5 mm. For comparison, pristine ceramic membranes were synthesized by a similar method without adding any Co_3O_4.

2.4. Characterization

The characterization of prepared materials was done using scanning electron microscopy (SEM) combined with energy dispersive X-Ray (EDS), X-ray diffraction (XRD), transmission electron microscopy (TEM) and high angle annular dark field scanning transmission electron microscopy (HAADF-STEM), atomic force microscopy (AFM), X-ray photoelectron spectroscopy (XPS), atomic emission spectroscopy (AES – leaching tests) and electron paramagnetic resonance (EPR). The detailed procedures for operations and equipment are explained in the supplementary information as Text S2.

2.5. Catalytic membrane oxidation of organic pollutants

The activity of Co@Al_2O_3 membrane was evaluated in a catalytic membrane reactor system (Fig. 1). The detailed procedure is explained

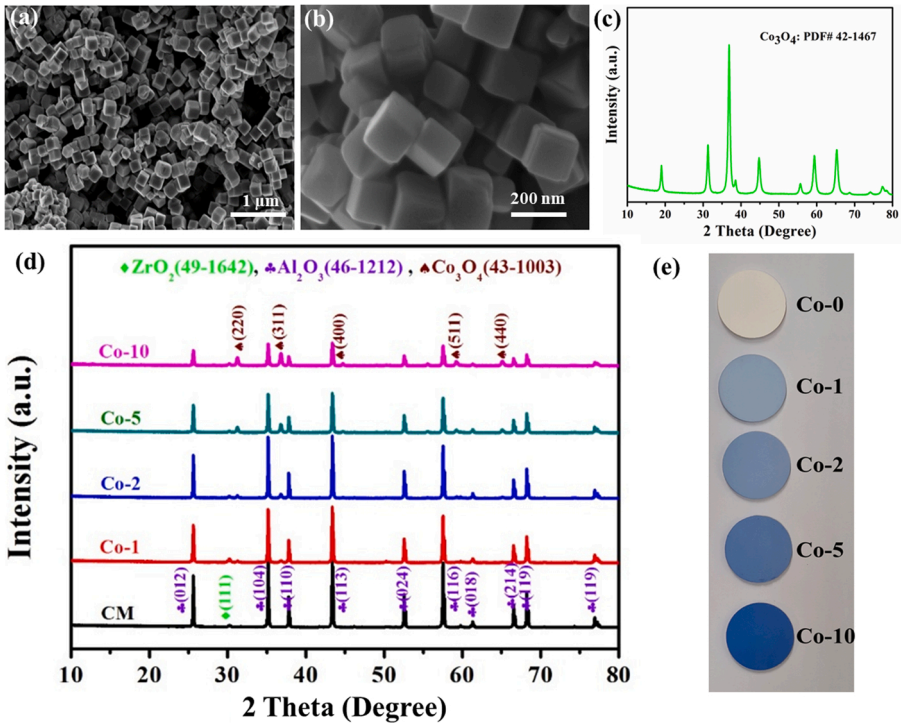

Fig. 2. (a and b) SEM images of Co-90–200 nanocubes, (c) XRD patterns of Co_3O_4 nanocubes, (d) XRD patterns of pristine and cobalt membranes and (e) Photos of pristine membrane and Co@Al_2O_3 catalytic membranes.

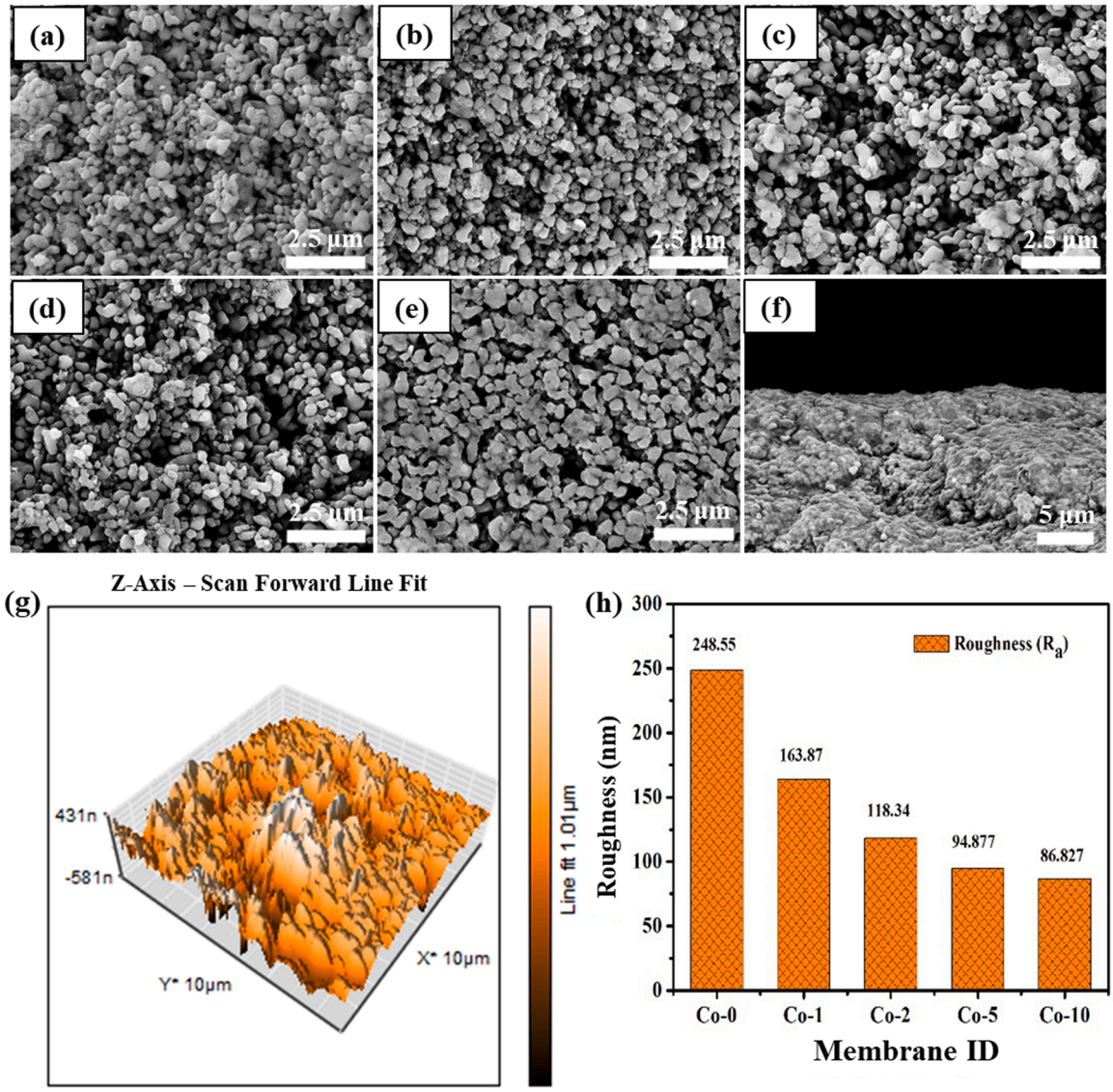

Fig. 3. SEM surface images of (a ~ e) pristine, Co-1, Co-2, Co-5 and Co-10 membranes, and cross-section image of (f) Co-5, (g) AFM image of Co-2 membrane and (h) the average roughness of the membranes.

in the supplementary information as Text S3.

2.6. Membrane fouling tests

The membrane fouling tests and the flux changes between various membranes were investigated in a closed dead-end membrane reactor. The detailed procedures of membrane fouling tests are explained in supplementary information as Text S4.

3. Results and discussion

3.1. Characterization of Co_3O_4 catalysts and Co@Al_2O_3 catalytic membranes

The properties of the Co_3O_4 nanocubes were first investigated. Fig. 2a and b show the SEM images of the Co_3O_4 nanocubes. Following the solvent-thermal and calcination process, the cubic-shaped Co_3O_4 catalysts with a size of about 200 nm were synthesized. Fig. 2c presents the XRD patterns of Co_3O_4 nanocubes. The diffraction peaks at 19.0, 31.3, 36.9, 38.5, 44.8, 55.7, 59.4, 65.2, 68.6, 74.1, and 77.3° were respectively denoted to the (111), (220), (311), (222), (400), (422), (511), (440), (531), (620), and (533) planes of Co_3O_4 (JCPDS NO. 42–1467, a = b = c = 8.084 Å) [34]. No other crystalline phases were observed, owing to the high purity of the catalysts. Fig. 2d shows the XRD patterns of the synthesised membranes. Diffraction peaks at 25.6, 35.2, 37.8, 43.4, 52.5, 57.5, 61.1, 61.3, 66.5, 68.2, 76.9 and 77.2°, were indexed to the (012), (104), (110), (113), (024), (116), (018), (122), (214), (300), (1010) and (119) planes of the Al_2O_3 support [35]. The other peaks at 31.3, 36.9, 44.8, 59.4, and 65.2° represented the (220), (311), (400), (511) and (440) planes of Co_3O_4. The results show that the Co_3O_4 phase remained unchanged after the high-temperature calcination. The peak at 30.1° was the (110) plane of ZrO_2 (JCPDS No.49–1642, a = b = c = 5.128 Å, α = β = γ = 90°) which came from the ZrO_2 milling balls and jar during the ball-milling process [36]. It can also be noticed that the intensity of Co_3O_4 peaks increased on the higher Co loading membrane samples. The photos of pristine CM and Co@Al_2O_3 with different Co loadings are shown in Fig. 2e.

The surface morphologies of the pristine Al_2O_3 membrane, Co-1, Co-2, Co-5, and Co-10 membranes are displayed in Fig. 3a, b, c, d and e, respectively. Fig. 3f shows a cross-section image of the Co-5 membrane. No significant change was observed in the surface morphology with increase in the cobalt loading. However, when high magnification

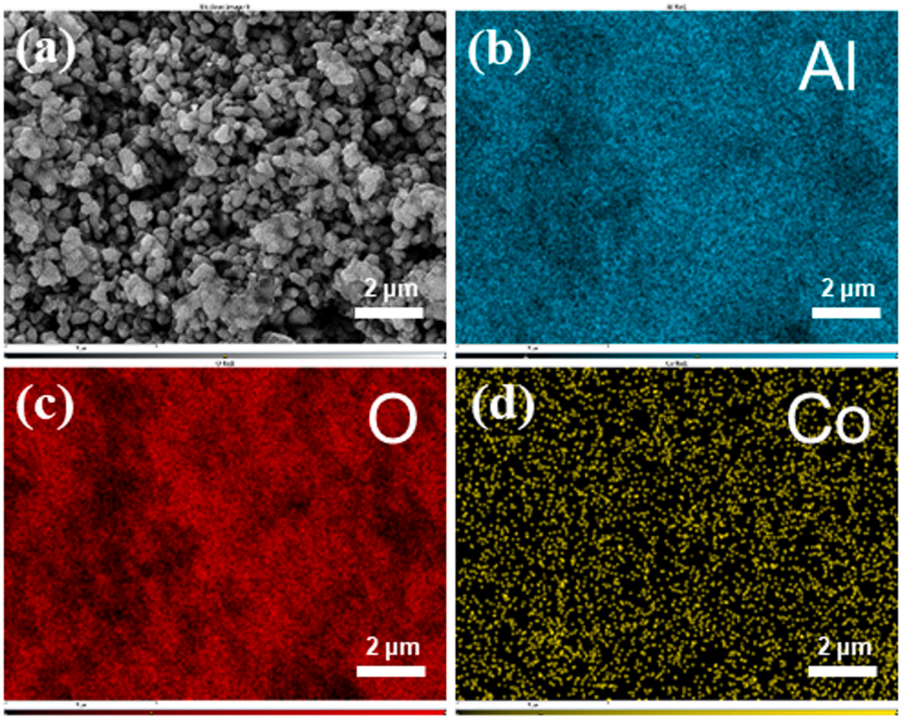

Fig. 4. (a) SEM image of Co-2 membrane, (b-d) corresponding elemental maps.

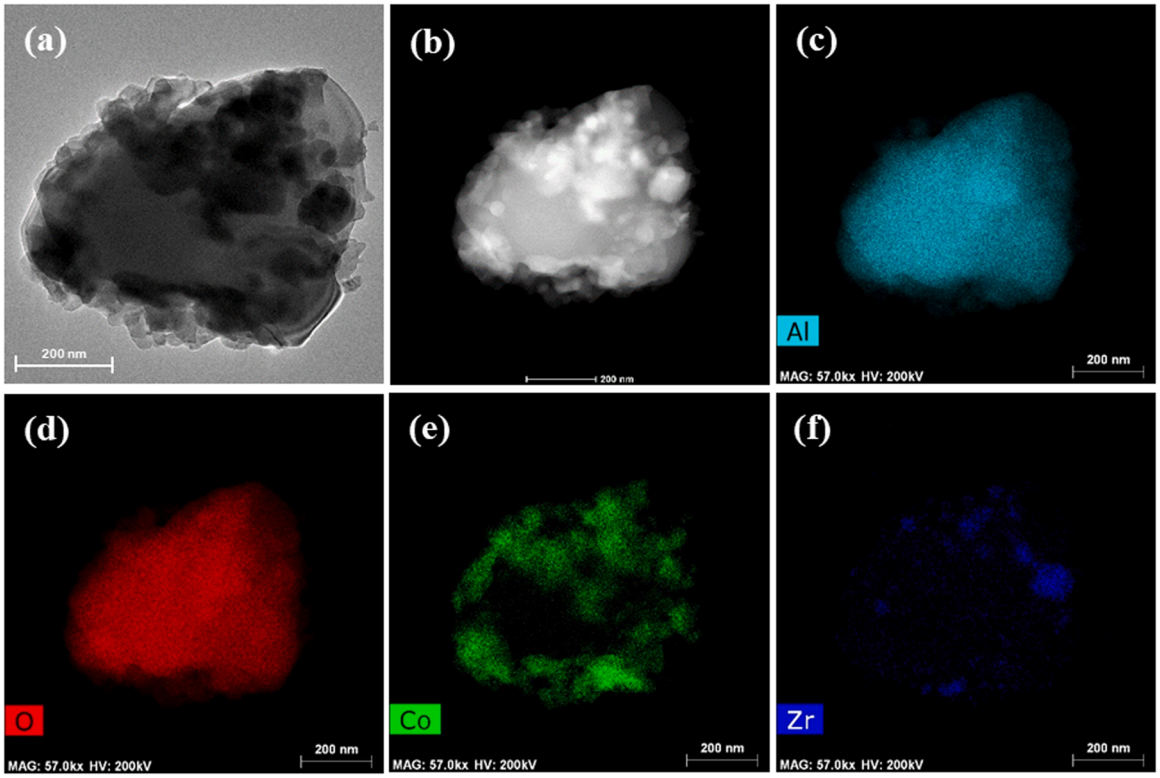

Fig. 5. (a) TEM image, (b) HAADF image of single Co-Al oxide grain (Co-2 membrane), and (c-f) mappings.

imaging was performed with AFM, it was found that the membrane surface became slightly smoother with an increase of Co loading in the Co@Al_2O_3 membranes. This is because Co_3O_4 has a melting point of 900 °C and would experience rearrangement during the calcination up to 1050 °C in the high-temperature muffle furnace [37].

The melted Co_3O_4 filled the pores and surface rough areas and made the high Co membrane smoother than the low Co loading catalytic membrane and the pristine CM. This can be further confirmed by AFM results (Figs. 3g and S1). Fig. 3h depicts the 3D surface topographies of the prepared membrane with different cobalt loading. Co-0 membrane exhibited a surface roughness of 248.55 nm followed by Co-1, Co-2, Co-5, and Co-10 with a surface roughness of 163.87, 118.34, 94.87 and

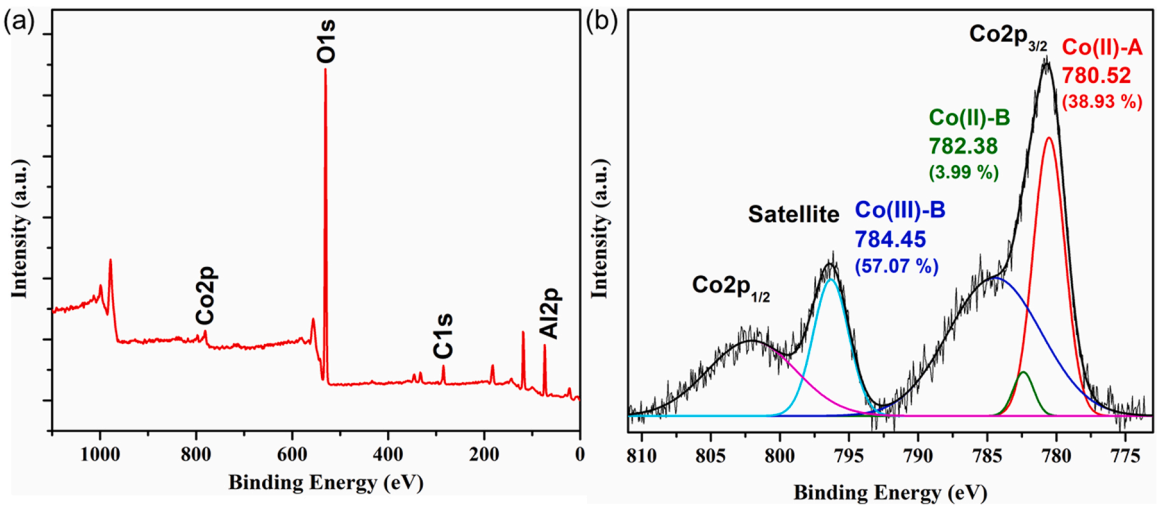

Fig. 6. (a) XPS survey scan of Co-2 membrane, (b) High resolution deconvoluted spectra of Co2P.

86.82 nm respectively.

Energy-dispersive x-ray spectroscopy (EDS) of the pristine CM and Co@Al_2O_3 catalytic membranes are shown in Fig. 4 and Figs.S2-S5, respectively. The elemental maps of indicate uniform distribution of Co_3O_4 on the membrane which can further be justified by the cross-sectional SEM-EDS mapping of Co-2 membrane (Fig. S6).

Fig. 5 shows a TEM image and elemental mapping of a single Co@Al_2O_3 particle from Co-2 membrane. The TEM (Fig. 5a) and HAADF-STEM (Fig. 5b) images of the particle reveal the relatively even distribution of the small Co_3O_4 nanoparticles on the Al_2O_3 particle which can further be justified by the elemental mapping (Fig. 5c-f). Fig. S7 reveals the element distribution spectrum of the Co-Al oxides. The uniform dispersion Co_3O_4 nanoparticles on Al_2O_3 in the composite ceramic catalytic membrane would provide reactive sites for the catalytic degradation. Further, this uniformity also aids in the uniform flow of the solution hence establishing an effective interaction of the PMS with Co_3O_4 nanoparticles leading to elevated degradation efficiencies. Zr was from the ZrO_2 milling balls and jar during the ball-milling process.

Fig. 6a shows the XPS survey scan of the Co-2 membrane. The scan reveals that Al, Co, O and adventitious C coexist in the membrane. The high resolution deconvoluted spectrum of Co2P is shown in Fig. 6b. Due to the spin-orbit coupling, the Co 2 P spectrum is split into $2p_{1/2}$ and $2p_{3/2}$ doublets with the addition of the satellite peaks. Two peaks at 780.52 and 782.38 eV correspond to a tetrahedral Co(II)-A site and an octahedral Co(II)-B site while the peak at 784.45 eV corresponds to a Co (III)-B site indicating the coexistence of Co^{3+} and Co^{2+} species in the Co-2 membrane [38,39]. The atomic ratio of Co^{2+}/Co^{3+} in the Co-2 membrane is calculated to be 0.75. This remarkably high atomic ratio could be attributed to the possible enrichment of the catalyst surface with abundant oxygen vacancies [40,41].

3.2. Catalytic oxidation of HBA

The degradation efficiencies of the as-prepared membranes were investigated through the oxidation of HBA (Fig. 7). After 30 min equilibrium time, 4 mM PMS was added to the feed solution. All the HBA samples were extracted from the permeate side and the concentrations were measured by HPLC. From this study, it can be noted that the use of catalytic membranes over the suspended particles would ease the catalyst's recovery from the solution [42]. Fig. 7a shows the effect of Co_3O_4 loading on HBA removal by the catalytic membranes. It was found that the HBA degradation performance was enhanced with the increase of Co loading. The increase in the degradation efficiency could be ascribed to the increased number of active sites which would increase the number of active species produced [38]. The pristine CM showed no significant degradation ability on HBA in the presence of PMS. When the Co-1 membrane was employed, complete HBA degradation was observed for the first 30 min. However, after 30 min the degradation efficiency started reducing as seen in Fig. 7a. This is because the Co content is too low in the Co-1 catalytic membrane and after 30 min reaction, most of the Co active sites were occupied by the HBA and the degradation intermediates. When Co loading is increased from 1% to 2%, the catalytic efficiency increases, and complete degradation is achieved even after 40 min. The results remain the same when the loading is further increased to 5% and 10%. This could be because the active radicals had been generated to a maximum degree from the activation of PMS [43,44]. As such, the Co-2 membrane is the most economical option in the Co@A_2O_3 membrane/PMS system. Further, cobalt ion leaching was tested on ICP after each run over different Co-loaded membranes. Fig. S8 shows the cobalt leaching contents over various membrane types. It can be noted that very low leaching levels were observed in all types of membranes suggesting their feasibility. The Co leaching content was in the order of Co-1 (0.34 mg/L) < Co-2 (0.93 mg/L) < Co-5 (1.67 mg/L) < Co-10 (2.11 mg/L).

The influence of the initial HBA concentration was also evaluated and different concentrations of HBA (10, 20, 50, and 100 ppm) were applied on the feed-in side (Fig. 7b). Results show that complete degradation in the permeate side can be only reached at low initial HBA concentrations (10 and 20 ppm). At high HBA concentrations (50 and 100 ppm), the HBA concentration at the permeate side sharply decreased and then gradually increased as the reaction continued, indicating a deteriorated catalytic ability of the Co@Al_2O_3 membrane when treating the high concentration of organic pollutants. This can be explained by the constant number of radicals generated with a fixed amount of catalyst loading and PMS loading. In order to achieve complete removal of HBA, more radicals are essential [45]. Fig. 7c shows the effect of PMS on HBA degradation. It was found that the Co-2 catalytic membrane itself has no degradation ability on HBA without PMS. The HBA degradation efficiency increased with an increase in PMS loading. This could be explained by the generation of more active radicals with the increase in PMS concentration [46]. When further increasing the PMS loading from 4 to 8 mM, no significant change was observed in the degradation efficiency. This is because the generation of excess $^{\bullet}OH$ and $SO_4^{\bullet-}$ would be consumed unfavorably resulting in the formation of HSO_4^- and $SO_5^{\bullet-}$ which are less reactive [47]. Therefore, 4 mM is the best PMS loading in the Co@Al_2O_3 catalytic membrane/PMS system.

In the heterogeneous activation of PMS, pH is a key factor. The pH influence on HBA degradation in the catalytic membrane/PMS system was also tested. Results reveal that the degradation ability of HBA

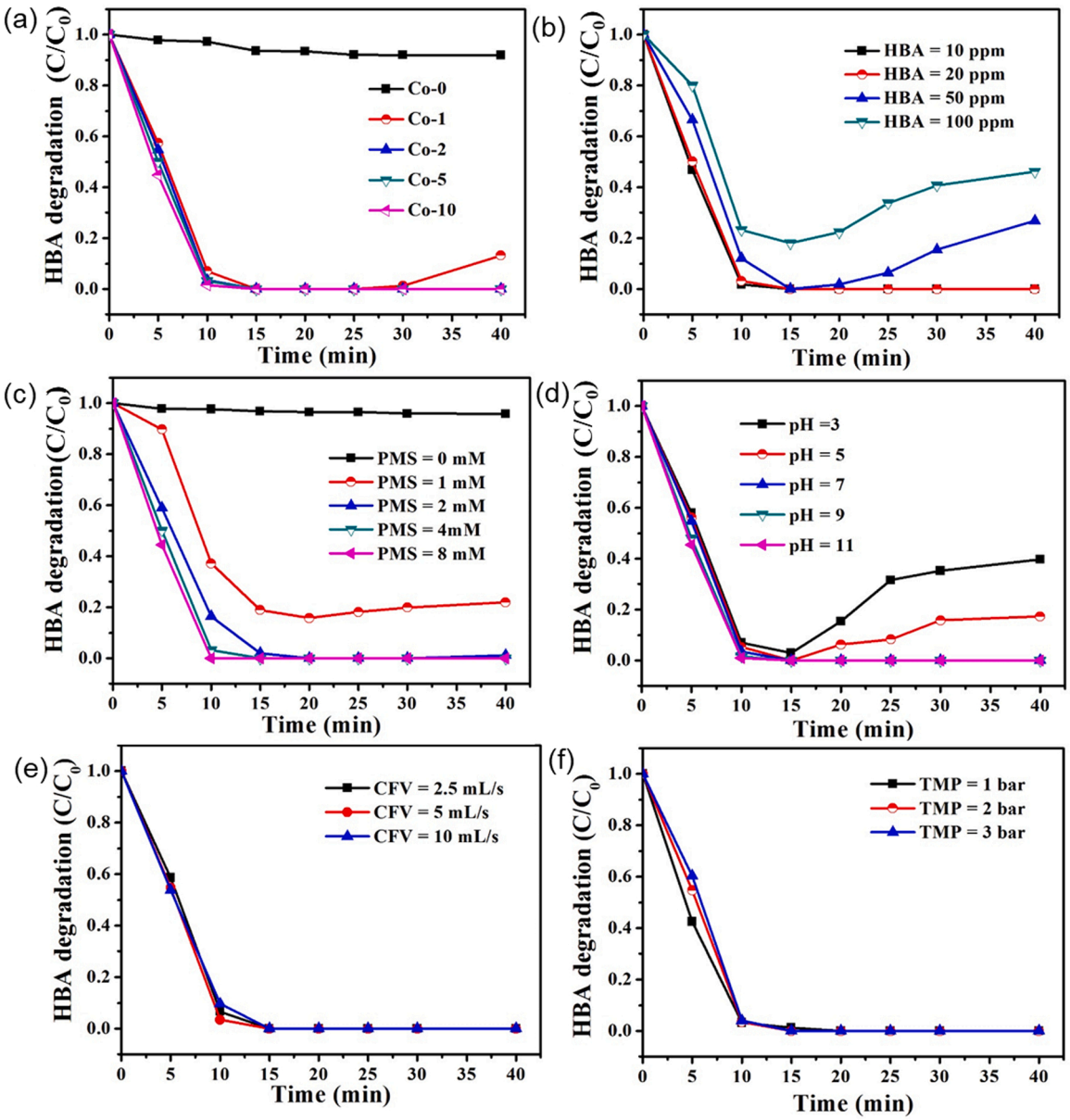

Fig. 7. Effect of different conditions on the degradation of HBA (a) catalysts loading, (b) initial HBA concentration, (c) PMS dosage, (d) initial pH, (e) CFV, and (f) TMP. Conditions: Co-2 membrane (b-f), [PMS] = 4 mM (for a-b, and d-f), TMP = 2 bar (for a-e), CFV = 5 mL s^{-1} (for a-d, and f), $[HBA]_0$ = 20 ppm (for a and c-f), and pH = 7 (for a-c and e, f).

dropped under acidic conditions (Fig. 7d). Much better degradation performance can be achieved in alkaline conditions. This could be due to the low stability of PMS at low pH. PMS has a pKa of 9.4 and therefore, at a lower pH, it is usually in the form of H_2SO_4 making it inert to be activated [48]. Further at higher pH, PMS can undergo self decomposition thereby making higher pH desirable for degradation [49]. No significant improvement in degradation rate was observed when the pH of the feed-in solution increased from 7 to 11. In addition, the cross-flow velocity (CFV) has a negligible influence on HBA degradation (Fig. 7e). However, the HBA degradation was found to be more effective at a lower transmembrane pressure (TMP) (Fig. 7f). This is because, at a lower TMP, the flow rate at the permeate side was lower, thus the contact time of the HBA/PMS mixed solution with the Co reactive sites on Co@Al_2O_3 increased.

3.3. Mechanistic study

To understand the HBA degradation mechanism and the generated ROSs in the Co@Al_2O_3 membrane/PMS system, both EPR and selective radical quenching tests were performed. As shown in Fig. 8a, both DMPO-$SO_4^{\bullet}$– and DMPO-$^{\bullet}OH$ adducts characteristic peaks are identified, suggesting the presence of $SO_4^{\bullet-}$ and $^{\bullet}OH$ radicals in the Co@Al_2O_3 membrane/PMS system [50,51]. From the EPR spectra in Fig. 8a, it can be seen that in the first 10 min, a large quantity of both sulphate and hydroxyl radicals are produced which then decreases as the reaction continues. This could be attributed to the high redox potential of both radicals whereby the radicals would react with HBA quickly hence leading to a decline in the intensities [52]. In addition, the interconversion between the two radicals and their gradual consumption would result in a decline in the intensities [50,53].

Further, selective radical quenching tests were carried out for the identification of the dominating species. Ethanol (EtOH) and tert-butyl alcohol (TBA) were used as the scavenging agents. EtOH is effective in scavenging both $^{\bullet}OH$ and $SO_4^{\bullet-}$ while TBA is employed to quench $^{\bullet}OH$ radicals [54,55]. The reaction rate of TBA (without α-H) with the $SO_4^{\bullet-}$ is much slower than that of EtOH (with α-H). As shown in Fig. 8b, EtOH

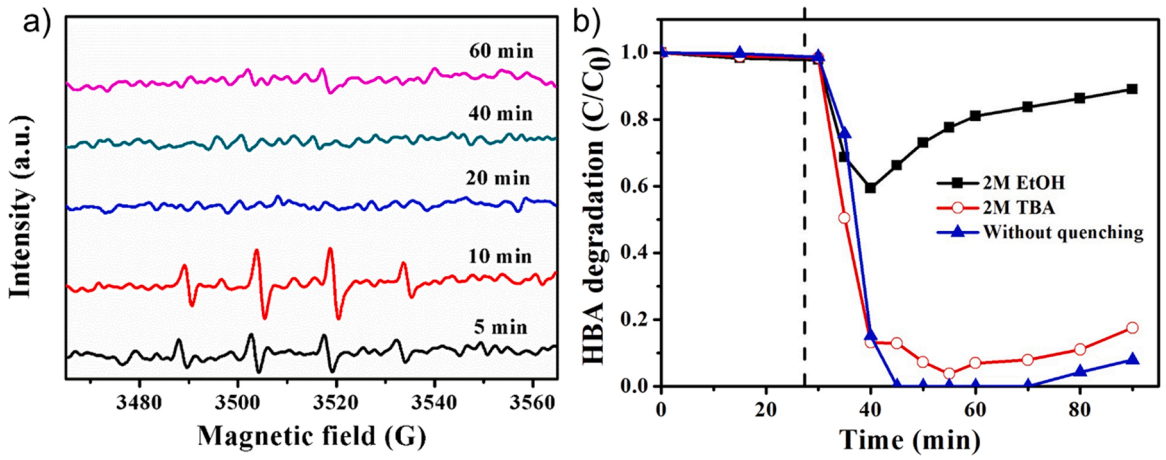

Fig. 8. (a) DMPO spin trapping EPR spectra of $Co@Al_2O_3$ membrane/PMS system. (b) Effects of EtOH and TBA on the degradation of HBA in the $Co@Al_2O_3$ membrane/PMS system. Conditions: Co-1 membrane, [PMS] = 4 mM, $[HBA]_0$ = 20 ppm, pH = 7, TMP = 2 bar, CFV = 5 mL s^{-1}, TBA = EtOH = 2 M.

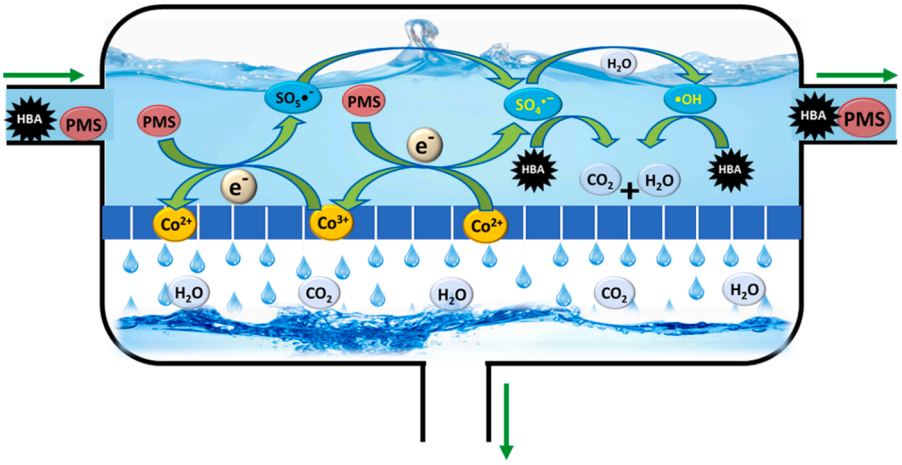

Fig. 9. Proposed mechanism for HBA degradation by the Co-2/PMS system.

had a significant effect on HBA degradation while TBA showed a minimal effect, suggesting that the sulfate radicals are the prominent ROSs in the $Co@Al_2O_3$ membrane/PMS system [56].

The activation of PMS is based on single-electron transfer reactions between Co^{2+} and Co^{3+} on the redox active surface of the Co-2 membrane as depicted in Eqs. (1) and (2) [57]. The redox reaction generates freely diffusible $SO_4^{\bullet-}$ which further reacts with OH^- or H_2O to produce $^{\bullet}OH$ as shown in Eqs. (3) and (4) [38,57]. In addition, Co^{3+} can further be reduced to a bivalent form (Co^{2+}) in the presence of PMS (Eq. (5)) resulting in the formation of $SO_5^{\bullet-}$ which can subsequently form

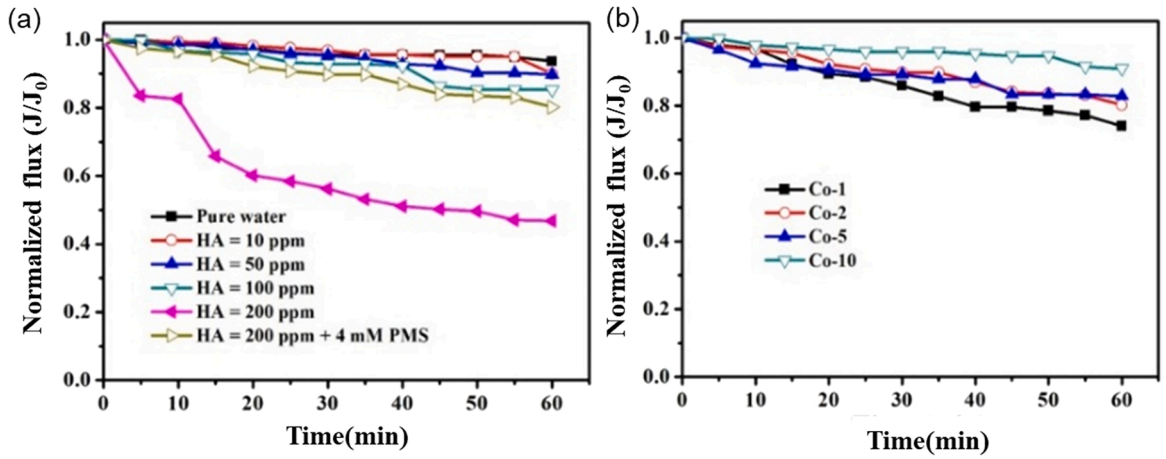

Fig. 10. Specific flux of (a) Co-2 membrane at different HA concentrations without or with 4 mM PMS, (b) different Co loading $Co@Al_2O_3$ membranes at 200 ppm HA solution with 4 mM PMS.

$SO_4^{\bullet-}$ (Eq. (6)) [58,59,57]. Finally, HBA molecules in the solution can be oxidized to small intermediates, CO_2 and H_2O by the effective attacking of the free radicals as depicted in Eq. (7). As reported in previous studies, it can be proposed that mineralisation of HBA could lead to the formation of two known intermediates, p-benzoquinone and hydroquinone as shown in Fig. S9, which could further be attacked by the active radicals to form simpler compounds [22,49]. Based on the discussions above, the proposed mechanism for HBA degradation by the Co-2/PMS system is presented in Fig. 9.

$$\equiv Co^{2+} + HSO_5^- \rightarrow \equiv Co^{3+} + SO_4^{\bullet-} + OH^- \quad (1)$$

$$\equiv Co^{2+} + HSO_5^- \rightarrow \equiv Co^{3+} + SO_4^- + {}^{\bullet}OH \quad (2)$$

$$SO_4^{\bullet-} + OH^- \rightarrow {}^{\bullet}OH + SO_4^{2-} \quad (3)$$

$$SO_4^{\bullet-} + H_2O \rightarrow HSO_4^- + {}^{\bullet}OH \quad (4)$$

$$\equiv Co^{3+} + HSO_5^- \rightarrow \equiv Co^{2+} + SO_5^{\bullet-} + H^+ \quad (5)$$

$$SO_5^{\bullet-} \rightarrow 2\ SO_4^{\bullet-} + O_2 \quad (6)$$

$$SO_4^{\bullet-} / {}^{\bullet}OH + HBA \rightarrow \{\ldots \text{multiple steps} \ldots\} \rightarrow \text{Intermediates} + CO_2 + H_2O \quad (7)$$

3.4. Fouling control evaluation

Despite having great waste treatment properties, membranes have a major concern of fouling. Various methods have been used in previous studies to mitigate membrane fouling such as in-situ treatment and pre-treatment, among others [16,60]. Cheng et al. studied membrane fouling using the pre-treatment method by using an Fe(II)/PMS system which showed a 70% reduction in the fouling [61]. Herein, PMS addition is used as a pretreatment to reduce membrane fouling as a result of organic matterAs displayed in Fig. 10a, it can be noted that when the PMS is not added as pre-treatment, the flux declined as the initial concentration of HAs increased. A significant membrane fouling is noted when 200 ppm HA is added to the feed-in solution. However, the addition of 4 mM PMS in the pre-treatment process can significantly reduce the fouling problem of Co-2 from 0.45 to 0.8 in 60 min Fig. 10b shows the membrane fouling alleviation performance of $Co@Al_2O_3$ membranes/PMS system by using different Co loading membranes (PMS = 4 mM and TMP = 1 bar). The results indicated that the order of flux decline extent in 1 h was as: Co-1 > Co-2 > Co-5 > Co-10. This can be explained by a higher level of ROSs generated when using a higher loading of Co catalytic membrane in the $Co@Al_2O_3$ membrane/PMS system.

4. Conclusion

In summary, nano-structured Co_3O_4/Al_2O_3 composite ceramic catalytic membranes were prepared by a simple milling and calcination process. The ball-milling technique helps with not only the formation of stable membrane but also the uniform dispersion of Co_3O_4 nanoparticles on the surface of Al_2O_3. $Co@Al_2O_3$ membranes with different Co catalytic membranes (Co_3O_4 weight ratio = 1, 2, 5, or 10%) were synthesized and the catalytic degradation of HBA was performed and optimised. The even distribution of Co_3O_4 catalyst in the membrane enhanced the generation of $SO_4^{\bullet-}$, endowing the $Co@Al_2O_3$ membranes with excellent catalytic performance for wastewater treatment. The HBA degradation performance was enhanced when using higher Co loading of $Co@Al_2O_3$ membranes. However, there is no significant improvement when Co loading is above 2%. The HBA degradation performances are also affected by initial PMS amount and solution pH values. The results revealed that the HBA degradation rate is higher at increased PMS loadings, while the improvement was not prominent when the PMS concentration exceeds 4 mM. It was also found that the $Co@Al_2O_3$ membrane/PMS system is more effective in neutral and alkaline conditions. In addition, the influences of cross-flow velocity and transmembrane pressure were also analysed. The results indicated that the $Co@Al_2O_3$ membranes/PMS system is not sensitive to the CFV. However, by decreasing the TMP, the degradation efficiency will be increased. This is because a lower TMP can keep a lower flow rate at the permeate side, resulting in a longer contact time of the HBA/PMS mix solution with the Co reactive sites on/ in the $Co@Al_2O_3$ membrane. EPR and selective radical quenching tests were performed to identify the reaction mechanism for HBA oxidation which depicted the presence of both $SO_4^{\bullet-}$, and •OH were active species in the catalytic membrane process with $SO_4^{\bullet-}$ as the dominant species. The anti-fouling performances of the $Co@Al_2O_3$ membranes/PMS system were also evaluated with HAs as the target foulant. Results indicated that the $Co@Al_2O_3$ membranes/PMS system played a synergistic role in treating HAs. With the addition of PMS, a great flux recovery was achieved even in a high HA content (200 ppm). This study provides a novel insight for integrating the Co_3O_4 catalysts with safe membrane technology in PMS activation for organic pollutants treatments.

CRediT authorship contribution statement

Rajan Arjan Kalyan Hirani: Conceptualization, Methodology, Investigation, Writing – original draft. **Hong Wu:** Methodology, Investigation, Formal analysis. **Abdul Hannan Asif:** Data curation. **Nasir Rafique:** Data curation. **Lei Shi:** Supervision, Resources. **Shu Zhang:** Supervision, Resources. **Zhentao Wu:** Supervision, Validation. **Lai-Chang Zhang:** Supervision, Validation. **Shaobin Wang:** Supervision. **Yu Yin:** Supervision. **Martin Saunders:** Data curation. **Hongqi Sun:** Supervision, Resources, Project administration, Writing – review & editing.

Declaration of Competing Interest

The authors declare that they have no known competing financial interests or personal relationships that could have appeared to influence the work reported in this paper.

Data availability

Data will be made available on request.

Acknowledgments

The author (Sun) would like to express his thanks for the supports from “Significant Research Achievement Award” from the Office of Deputy Vice-Chancellor Research, Edith Cowan University. The authors acknowledge the facilities, and the scientific and technical assistance provided by A. Suvorova, H. Li and L. Kirilak of Microscopy Australia at the Centre for Microscopy, Characterisation & Analysis, The University of Western Australia, a facility funded by the University, State and Commonwealth Governments.

Appendix A. Supporting information

Supplementary data associated with this article can be found in the online version at doi:10.1016/j.jhazmat.2023.130874.

References

[1] Duan, X., Sun, H., Kang, J., Wang, Y., Indrawirawan, S., Wang, S., 2015. Insights into heterogeneous catalysis of persulfate activation on dimensional-structured nanocarbons. ACS Catal. 5 (8), 4629–4636. https://doi.org/10.1021/acscatal.5b00774.

[2] Kang, J., Zhou, L., Duan, X., Sun, H., Wang, S., 2018. Catalytic degradation of antibiotics by metal-free catalysis over nitrogen-doped graphene. Catal Today. https://doi.org/10.1016/j.cattod.2018.12.002.

[3] Duan, X., Sun, H., Wang, S., 2018. Metal-free carbocatalysis in advanced oxidation reactions. Acc Chem Res 51 (3), 678–687. https://doi.org/10.1021/acs.accounts.7b00535.

[4] Kang, J., Duan, X., Wang, C., Sun, H., Tan, X., Tade, M.O., Wang, S., 2018. Nitrogen-doped bamboo-like carbon nanotubes with Ni encapsulation for persulfate activation to remove emerging contaminants with excellent catalytic stability. Chem Eng J 332, 398–408. https://doi.org/10.1016/j.cej.2017.09.102.

[5] Sun, H., Wang, S., 2015. Catalytic oxidation of organic pollutants in aqueous solution using sulfate radicals. Catalysis 27, 209–247.

[6] Duan, X., Su, C., Miao, J., Zhong, Y., Shao, Z., Wang, S., Sun, H., 2018. Insights into perovskite-catalyzed peroxymonosulfate activation: Maneuverable cobalt sites for promoted evolution of sulfate radicals. Appl Catal B: Environ 220, 626–634. https://doi.org/10.1016/j.apcatb.2017.08.088.

[7] Duan, X., Sun, H., Ao, Z., Zhou, L., Wang, G., Wang, S., 2016. Unveiling the active sites of graphene-catalyzed peroxymonosulfate activation. Carbon 107, 371–378. https://doi.org/10.1016/j.carbon.2016.06.016.

[8] Wang, J., Wang, S., 2018. Activation of persulfate (PS) and peroxymonosulfate (PMS) and application for the degradation of emerging contaminants. Chem Eng J 334, 1502–1517. https://doi.org/10.1016/j.cej.2017.11.059.

[9] Ghanbari, F., Moradi, M., 2017. Application of peroxymonosulfate and its activation methods for degradation of environmental organic pollutants: Review. Chem Eng J 310, 41–62. https://doi.org/10.1016/j.cej.2016.10.064.

[10] Anipsitakis, G.P., Dionysiou, D.D., 2004. Radical generation by the interaction of transition metals with common oxidants. Environ Sci Technol 38 (13), 3705–3712. https://doi.org/10.1021/es035121o.

[11] Hu, P., Long, M., 2016. Cobalt-catalyzed sulfate radical-based advanced oxidation: A review on heterogeneous catalysts and applications. Appl Catal B: Environ 181, 103–117. https://doi.org/10.1016/j.apcatb.2015.07.024.

[12] Saputra, E., Muhammad, S., Sun, H., Ang, H.-M., Tadé, M.O., Wang, S., 2014. Shape-controlled activation of peroxymonosulfate by single crystal α-$Mn_2O_3$for catalytic phenol degradation in aqueous solution. Appl Catal B: Environ 154–155, 246–251. https://doi.org/10.1016/j.apcatb.2014.02.026.

[13] Kang, J., Zhang, H., Duan, X., Sun, H., Tan, X., Wang, S., 2019. Nickel in hierarchically structured nitrogen-doped graphene for robust and promoted degradation of antibiotics. J Clean Prod 218, 202–211. https://doi.org/10.1016/j.jclepro.2019.01.323.

[14] Duan, X., Tian, W., Zhang, H., Sun, H., Ao, Z., Shao, Z., Wang, S., 2019. sp2/sp3 framework from diamond nanocrystals: a key bridge of carbonaceous structure to carbocatalysis. ACS Catal. 9 (8), 7494–7519. https://doi.org/10.1021/acscatal.9b01565.

[15] Oh, W.-D., Dong, Z., Lim, T.-T., 2016. Generation of sulfate radical through heterogeneous catalysis for organic contaminants removal: Current development, challenges and prospects. Appl Catal B: Environ 194, 169–201. https://doi.org/10.1016/j.apcatb.2016.04.003.

[16] Cheng, X., Liang, H., Ding, A., Zhu, X., Tang, X., Gan, Z., Xing, J., Wu, D., Li, G., 2017. Application of Fe(II)/peroxymonosulfate for improving ultrafiltration membrane performance in surface water treatment: Comparison with coagulation and ozonation. Water Res 124, 298–307. https://doi.org/10.1016/j.watres.2017.07.062.

[17] Fan, J., Lin, T., Chen, W., Xu, H., Tao, H., 2020. Control of ultrafiltration membrane fouling during the recycling of sludge water based on Fe(II)-activated peroxymonosulfate pretreatment. Chemosphere 246, 125840. https://doi.org/10.1016/j.chemosphere.2020.125840.

[18] Yang, M., Chen, J., Peng, B., Yu, Z., Chu, H., Zhou, X., 2019. Performance and properties of coking nanofiltration concentrate treatment and membrane fouling mitigation by an Fe(ii)/persulfate-coagulation-ultrafiltration process. RSC Adv 9 (27), 15277–15287. https://doi.org/10.1039/C8RA10094B.

[19] Cheng, X., Li, P., Liu, W., Luo, C., Wu, D., Zhou, W., Zheng, L., Zhu, X., Liang, H., 2020. Activation of peroxymonosulfate by metal oxide nanoparticles for mitigating organic membrane fouling in surface water treatment. Sep Purif Technol 246, 116935. https://doi.org/10.1016/j.seppur.2020.116935.

[20] Wang, S., Tian, J., Wang, Q., Xiao, F., Gao, S., Shi, W., Cui, F., 2019. Development of CuO coated ceramic hollow fiber membrane for peroxymonosulfate activation: a highly efficient singlet oxygen-dominated oxidation process for bisphenol a degradation. Appl Catal B: Environ 256, 117783. https://doi.org/10.1016/j.apcatb.2019.117783.

[21] Wang, S., Tian, J., Wang, Q., Zhao, Z., Cui, F., Li, G., 2019. Low-temperature sintered high-strength CuO doped ceramic hollow fiber membrane: Preparation, characterization and catalytic activity. J Membr Sci 570–571, 333–342. https://doi.org/10.1016/j.memsci.2018.10.078.

[22] Wu, H., Xu, X., Shi, L., Yin, Y., Zhang, L.-C., Wu, Z., Duan, X., Wang, S., Sun, H., 2019. Manganese oxide integrated catalytic ceramic membrane for degradation of organic pollutants using sulfate radicals. Water Res 167, 115110. https://doi.org/10.1016/j.watres.2019.115110.

[23] Zhao, Y., Lu, D., Xu, C., Zhong, J., Chen, M., Xu, S., Cao, Y., Zhao, Q., Yang, M., Ma, J., 2020. Synergistic oxidation - filtration process analysis of catalytic $CuFe_2O_4$ - Tailored ceramic membrane filtration via peroxymonosulfate activation for humic acid treatment. Water Res 171, 115387. https://doi.org/10.1016/j.watres.2019.115387.

[24] Pedrosa, M., Drazic, G., Tavares, P.B., Figueiredo, J.L., Silva, A.M.T., 2019. Metal-free graphene-based catalytic membrane for degradation of organic contaminants by persulfate activation. Chem Eng J 369, 223–232. https://doi.org/10.1016/j.cej.2019.02.211.

[25] Sheng, J., Yin, H., Qian, F., Huang, H., Gao, S., Wang, J., 2020. Reduced graphene oxide-based composite membranes for in-situ catalytic oxidation of sulfamethoxazole operated in membrane filtration. Sep Purif Technol 236, 116275. https://doi.org/10.1016/j.seppur.2019.116275.

[26] Anipsitakis, G.P., Dionysiou, D.D., 2003. Degradation of organic contaminants in water with sulfate radicals generated by the conjunction of peroxymonosulfate with cobalt. Environ Sci Technol 37 (20), 4790–4797. https://doi.org/10.1021/es0263792.

[27] Anipsitakis, G.P., Dionysiou, D.D., 2004. Transition metal/UV-based advanced oxidation technologies for water decontamination. Appl Catal B: Environ 54 (3), 155–163. https://doi.org/10.1016/j.apcatb.2004.05.025.

[28] Li, P., Ding, D., Salvi, R., Roth, J.A., 2015. Cobalt-induced ototoxicity in rat postnatal cochlear organotypic cultures. Neurotox Res 28 (3), 209–221. https://doi.org/10.1007/s12640-015-9538-8.

[29] Bao, Y., Lim, T.-T., Wang, R., Webster, R.D., Hu, X., 2018. Urea-assisted one-step synthesis of cobalt ferrite impregnated ceramic membrane for sulfamethoxazole degradation via peroxymonosulfate activation. Chem Eng J 343, 737–747. https://doi.org/10.1016/j.cej.2018.03.010.

[30] Bao, Y., Tian, M., Lua, S.K., Lim, T.-T., Wang, R., Hu, X., 2020. Spatial confinement of cobalt crystals in carbon nanofibers with oxygen vacancies as a high-efficiency catalyst for organics degradation. Chemosphere 245, 125407. https://doi.org/10.1016/j.chemosphere.2019.125407.

[31] Wang, Z., Nengzi, L.-c, Zhang, X., Zhao, Z., Cheng, X., 2020. Novel $NiCo_2S_4$/CS membranes as efficient catalysts for activating persulfate and its high activity for degradation of nimesulide. Chem Eng J 381, 122517. https://doi.org/10.1016/j.cej.2019.122517.

[32] Zhao, Q., Lu, D., Jiang, H., Zhao, Y., Sun, Y., Li, Z., Yang, M., Wang, P., Ma, J., 2018. Peroxymonosulfate-based cleaning technology for metal oxide-coated ceramic ultrafiltration membrane polluted by Alcian Blue 8GX dye: Radical and non-radical oxidation cleaning mechanism. J Membr Sci. https://doi.org/10.1016/j.memsci.2018.11.057.

[33] Song, H., Shen, L., Wang, C., 2014. Template-free method towards quadrate Co_3O_4 nanoboxes from cobalt coordination polymer nano-solids for high performance lithium ion battery anodes. J Mater Chem A 2 (48), 20597–20604. https://doi.org/10.1039/C4TA04252B.

[34] Lv, Y., Li, Y., Shen, W., 2013. Synthesis of Co_3O_4 nanotubes and their catalytic applications in CO oxidation. Catal Commun 42, 116–120. https://doi.org/10.1016/j.catcom.2013.08.017.

[35] Chai, R., Chen, P., Zhang, Z., Zhao, G., Liu, Y., Lu, Y., 2017. Thin-felt NiO-Al_2O_3/FeCrAl-fiber catalyst for high-throughput catalytic oxy-methane reforming to syngas. Catal Commun 101, 48–50. https://doi.org/10.1016/j.catcom.2017.07.023.

[36] Jing, P., Liu, M., Wang, P., Yang, J., Tang, M., He, C., Pu, Y., Liu, M., 2020. Flexible nonwoven ZrO_2 ceramic membrane as an electrochemically stable and flame-resistant separator for high-power rechargeable batteries. Chem Eng J 388, 124259. https://doi.org/10.1016/j.cej.2020.124259.

[37] Kang, Y.-M., Kim, K.-T., Kim, J.-H., Kim, H.-S., Lee, P.S., Lee, J.-Y., Liu, H.K., Dou, S.X., 2004. Electrochemical properties of Co_3O_4, Ni–Co_3O_4 mixture and Ni–Co_3O_4 composite as anode materials for Li ion secondary batteries. J Power Sources 133 (2), 252–259. https://doi.org/10.1016/j.jpowsour.2004.02.012.

[38] Asif, A.H., Rafique, N., Hirani, R.A.K., Wu, H., Shi, L., Sun, H., 2021. Heterogeneous activation of peroxymonosulfate by Co-doped Fe_2O_3 nanospheres for degradation of p-hydroxybenzoic acid. J Colloid Interface Sci 604, 390–401. https://doi.org/10.1016/j.jcis.2021.06.161.

[39] Li, P., Zeng, H.C., 2017. Sandwich-like nanocomposite of CoNiOx/reduced graphene oxide for enhanced electrocatalytic water oxidation. Adv Funct Mater 27 (13), 1606325. https://doi.org/10.1002/adfm.201606325.

[40] Li, L., Wu, H., Chen, H., Zhang, J., Xu, X., Wang, S., Sun, H., 2020. Heterogeneous activation of peroxymonosulfate by hierarchically porous cobalt/iron bimetallic oxide nanosheets for degradation of phenol solutions. Chemosphere 256, 127160. https://doi.org/10.1016/j.chemosphere.2020.127160.

[41] Li, P., Lin, Y., Zhao, S., Fu, Y., Li, W., Chen, R., Tian, S., 2021. Defect-engineered Co_3O_4 with porous multishelled hollow architecture enables boosted advanced oxidation processes. Appl Catal B: Environ 298, 120596. https://doi.org/10.1016/j.apcatb.2021.120596.

[42] Zhang, S., Hedtke, T., Zhu, Q., Sun, M., Weon, S., Zhao, Y., Stavitski, E., Elimelech, M., Kim, J.-H., 2021. Membrane-confined iron oxychloride nanocatalysts for highly efficient heterogeneous fenton water treatment. Environ Sci Technol 55 (13), 9266–9275. https://doi.org/10.1021/acs.est.1c01391.

[43] Chen, F., Huang, G.-X., Yao, F.-B., Yang, Q., Zheng, Y.-M., Zhao, Q.-B., Yu, H.-Q., 2020. Catalytic degradation of ciprofloxacin by a visible-light-assisted peroxymonosulfate activation system: Performance and mechanism. Water Res 173, 115559. https://doi.org/10.1016/j.watres.2020.115559.

[44] Luo, J., Bo, S., Qin, Y., An, Q., Xiao, Z., Zhai, S., 2020. Transforming goat manure into surface-loaded cobalt/biochar as PMS activator for highly efficient ciprofloxacin degradation. Chem Eng J 395, 125063. https://doi.org/10.1016/j.cej.2020.125063.

[45] Hong, Y., Peng, J., Zhao, X., Yan, Y., Lai, B., Yao, G., 2019. Efficient degradation of atrazine by CoMgAl layered double oxides catalyzed peroxymonosulfate: Optimization, degradation pathways and mechanism. Chem Eng J 370, 354–363. https://doi.org/10.1016/j.cej.2019.03.127.

[46] Huang, Z., Bao, H., Yao, Y., Lu, W., Chen, W., 2014. Novel green activation processes and mechanism of peroxymonosulfate based on supported cobalt phthalocyanine catalyst. Appl Catal B: Environ 154–155, 36–43. https://doi.org/10.1016/j.apcatb.2014.02.005.

[47] Zhuang, Y., Wang, X., Zhang, L., Dionysiou, D.D., Kou, Z., Shi, B., 2020. Double-network hydrogel templated FeS/graphene with enhanced PMS activation

performance: considering the effect of the template and iron species. Environ Sci: Nano 7 (3), 817–828. https://doi.org/10.1039/C9EN01391A.
[48] Dong, Q., Wang, J., Duan, X., Tan, X., Liu, S., Wang, S., 2019. Self-Assembly of 3D MNO2/N-doped graphene hybrid aerogel for catalytic degradation of water pollutants: Structure-dependent activity. Chem Eng J 369, 1049–1058. https://doi.org/10.1016/j.cej.2019.03.139.
[49] Hirani, R.A.K., Asif, A.H., Rafique, N., Wu, H., Shi, L., Zhang, S., Duan, X., Wang, S., Saunders, M., Sun, H., 2022. Three-dimensional nitrogen-doped graphene oxide beads for catalytic degradation of aqueous pollutants. Chem Eng J 446, 137042. https://doi.org/10.1016/j.cej.2022.137042.
[50] Gao, H., Yang, H., Xu, J., Zhang, S., Li, J., 2018. Strongly Coupled g-C_3N_4 Nanosheets-Co_3O_4 Quantum Dots as 2D/0D Heterostructure Composite for Peroxymonosulfate Activation. Small 14 (31), 1801353. https://doi.org/10.1002/smll.201801353.
[51] Zhou, X., Luo, C., Luo, M., Wang, Q., Wang, J., Liao, Z., Chen, Z., Chen, Z., 2020. Understanding the synergetic effect from foreign metals in bimetallic oxides for PMS activation: A common strategy to increase the stoichiometric efficiency of oxidants. Chem Eng J 381, 122587. https://doi.org/10.1016/j.cej.2019.122587.
[52] Wang, Y., Ao, Z., Sun, H., Duan, X., Wang, S., 2016. Activation of peroxymonosulfate by carbonaceous oxygen groups: experimental and density functional theory calculations. Appl Catal B: Environ 198, 295–302. https://doi.org/10.1016/j.apcatb.2016.05.075.
[53] Duan, X., Ao, Z., Sun, H., Indrawirawan, S., Wang, Y., Kang, J., Liang, F., Zhu, Z.H., Wang, S., 2015. Nitrogen-Doped Graphene for Generation and Evolution of Reactive Radicals by Metal-Free Catalysis. ACS Appl Mater Interfaces 7 (7), 4169–4178. https://doi.org/10.1021/am508416n.
[54] Wang, F., Xiao, M., Ma, X., Wu, S., Ge, M., Yu, X., 2021. Insights into the transformations of Mn species for peroxymonosulfate activation by tuning the Mn_3O_4 shapes. Chem Eng J 404, 127097. https://doi.org/10.1016/j.cej.2020.127097.
[55] Wang, Y., Sun, H., Ang, H.M., Tadé, M.O., Wang, S., 2015. 3D-hierarchically structured MnO_2 for catalytic oxidation of phenol solutions by activation of peroxymonosulfate: Structure dependence and mechanism. Appl Catal B: Environ 164, 159–167. https://doi.org/10.1016/j.apcatb.2014.09.004.
[56] Zhou, H., Peng, J., Li, J., You, J., Lai, L., Liu, R., Ao, Z., Yao, G., Lai, B., 2021. Metal-free black-red phosphorus as an efficient heterogeneous reductant to boost Fe^{3+}/Fe^{2+} cycle for peroxymonosulfate activation. Water Res 188, 116529. https://doi.org/10.1016/j.watres.2020.116529.
[57] Yu, Y., Ji, Y., Lu, J., Yin, X., Zhou, Q., 2021. Degradation of sulfamethoxazole by Co_3O_4-palygorskite composites activated peroxymonosulfate oxidation. Chem Eng J 406, 126759. https://doi.org/10.1016/j.cej.2020.126759.
[58] Abdul Nasir Khan, M., Kwame Klu, P., Wang, C., Zhang, W., Luo, R., Zhang, M., Qi, J., Sun, X., Wang, L., Li, J., 2019. Metal-organic framework-derived hollow Co_3O_4/carbon as efficient catalyst for peroxymonosulfate activation. Chem Eng J 363, 234–246. https://doi.org/10.1016/j.cej.2019.01.129.
[59] Deng, J., Feng, S., Zhang, K., Li, J., Wang, H., Zhang, T., Ma, X., 2017. Heterogeneous activation of peroxymonosulfate using ordered mesoporous Co_3O_4 for the degradation of chloramphenicol at neutral pH. Chem Eng J 308, 505–515. https://doi.org/10.1016/j.cej.2016.09.075.
[60] Asif, M.B., Zhang, Z., 2021. Ceramic membrane technology for water and wastewater treatment: A critical review of performance, full-scale applications, membrane fouling and prospects. Chem Eng J 418, 129481. https://doi.org/10.1016/j.cej.2021.129481.
[61] Cheng, X., Wu, D., Liang, H., Zhu, X., Tang, X., Gan, Z., Xing, J., Luo, X., Li, G., 2018. Effect of sulfate radical-based oxidation pretreatments for mitigating ceramic UF membrane fouling caused by algal extracellular organic matter. Water Res 145, 39–49. https://doi.org/10.1016/j.watres.2018.08.018.